# On the Quasi-Orthogonality of LoRa Modulation

Jae-Mo Kang, *Member, IEEE*, and Dong-Woo Lim

***Abstract*—Long Range (LoRa), a low power and wide-area modulation scheme based on chirp spread spectrum, is the most popular and widely adopted Internet of Things (IoT) technique in industry. A notable and interesting property of LoRa modulation is the quasi-orthogonality of signals modulated under different spreading factors (SFs). Unfortunately, in the literature, there has been no analytical effort to establish the theoretical validity of such quasi-orthogonality. This article, for the first time, theoretically tackles the quasi-orthogonality of the LoRa modulation. First, we derive in both continuous- and discrete-time domains the cross-correlation between two nonsynchronized LoRa signals with different SFs, based on which we analyze the quasi-orthogonality of the LoRa modulation and draw some useful engineering insights. Particularly, we analytically show that in the continuous-time domain, the quasi-orthogonality is guaranteed if one of the SFs of the two LoRa signals is large enough; while, in the discrete-time domain, the quasi-orthogonality is ensured if the maximum of the SFs is large enough. Furthermore, for practical values of the SF, the maximum squared magnitudes of the cross-correlation in the continuous- and discrete-time domains are shown to be 1.14% and 1.08%, respectively, compared to their peak values. We demonstrate the validity and accuracy of our analysis through extensive numerical simulations.**

***Index Terms*—Cross-correlation, Internet of Things (IoT), long-range (LoRa), performance analysis, quasi-orthogonality.**

## I. Introduction

INTERNET of Things (IoT) is a key enabling technology to realize anywhere and anytime connectivity for anyone and anything with a variety of applicability [1]. Low-power wide-area network (LPWAN) technologies are very promising and appealing for IoT as they offer long-range communications (e.g., over several kilometers) with extended battery lives [2]. Long Range (LoRa) is one of the most popular and widely adopted LPWAN technologies in industry, which adopts a chirp spread spectrum as its modulation scheme [3], [4], [5], [6]. LoRa is also promising for supporting vehicular communications such as vehicle-to-vehicle (V2V), vehicle-to-everything (V2X), and unmanned-aerial-vehicle-to-everything (U2X) communications [7].

A notable and intriguing feature of the LoRa modulation is that signals modulated under different spreading factors (SFs) are quasi-orthogonal (i.e., nearly orthogonal) [8], [9], [10]. Theoretically analyzing such quasi-orthogonality is very important in many practical/industrial applications with LoRa modulation to understand the fundamental performance limit and behavior of the system. Also, the quasi-orthogonality property is particularly useful and crucial for designs and performance analysis of LoRa networks [8], [9], [10]. However, in the literature, there has been no analytical effort to establish theoretical validity of the quasi-orthogonality of the LoRa modulation.

Recently, several efforts have been made to identify the cross-correlation of the LoRa signals modulated under the same SF [6], [11]; and the cross-correlation between up and down chirps modulated under the same SF [12]. However, the results obtained in [6], [11], and [12] are not applicable for theoretically establishing the quasi-orthogonality of the LoRa signals modulated under different SFs. Meanwhile, in [13] and [14], the impact of the quasi-orthogonality of the LoRa modulation has been investigated experimentally through numerical simulations, from which, however, it is not easy to obtain any theoretical insights. Moreover, none of the works in [13] and [14] give an (explicit) answer to the following important and fundamental question: under which conditions, the quasi-orthogonality of the LoRa modulation is established? and what is the analytical expression of the cross-correlation between the LoRa modulated signals with different SFs? To the best of our knowledge, this question still remains unanswered in the literature. This motivated our work.

In this article, we for the first time theoretically tackle the quasi-orthogonality of the LoRa modulation in both continuous- and discrete-time domains. Particularly, our thorough analysis identifies important conditions, under which two nonsynchronized LoRa signals modulated with different SFs are quasi-orthogonal. The main contributions of this article are summarized as follows.

1) We derive an analytical expression of the cross-correlation between two nonsynchronized continuous-time LoRa signals with different SFs in terms of Fresnel functions. It is also analytically shown that the quasi-orthogonality of the LoRa modulation is guaranteed in the continuous-time domain when one of the SFs of the two LoRa signals is large enough; and that for the practical values of the SF, the squared magnitude of the cross-correlation in the continuous-time domain ranges between 0.04% and 1.14% of the peak value.

Manuscript received 25 June 2022; revised 12 January 2023; accepted 9 February 2023. Date of publication 16 February 2023; date of current version 7 July 2023. This work was supported in part by the National Research Foundation of Korea (NRF) Grant funded by the South Korea Government (MSIT) under Grant 2022R1A4A1033830; in part by the Ministry of Science and ICT (MSIT), South Korea, through the Information Technology Research Center Support Program supervised by the Institute of Information and Communications Technology Planning and Evaluation (IITP) under Grant IITP-2023-2020-0-01808; and in part by the National Research Foundation (NRF), South Korea, under Project BK21 FOUR. *(Corresponding author: Dong-Woo Lim.)*

Jae-Mo Kang is with the Department of Artificial Intelligence, Kyungpook National University, Daegu 41566, South Korea (e-mail: jmkang@knu.ac.kr).

Dong-Woo Lim is with the Radio and Satellite Research Division, Electronics and Telecommunications Research Institute, Daejeon 34129, South Korea (e-mail: window0508@etri.re.kr).

Digital Object Identifier 10.1109/JIOT.2023.3245885

TABLE I
COMPARISONS OF OUR WORK AND RELATED WORKS

| | [6] and [11] | [12] | **Our work** |
|---|---|---|---|
| Approach | Derivation of cross-correlation between LoRa signals modulated under the same SF | Derivation of cross-correlation between up and down chirps modulated under the same SF | **Derivation of cross-correlation between LoRa signals modulated under different SFs** |
| Main finding | Analytical expressions for the cross-correlation between LoRa signals with the same SF | Analytical expressions for the cross-correlation between up and down chirps with the same SF | **Analytical expressions for the cross-correlation between LoRa signals with different SFs and conditions for the quasi-orthogonality** |
| Limitation | Inapplicability to theoretically establishing the quasi-orthogonality of the LoRa signals with different SFs | | |

2) We also derive an analytical expression of the cross-correlation between two nonsynchronized discrete-time LoRa signals in an exponential form and show that the quasi-orthogonality of the LoRa modulation is ensured in the discrete-time domain when the maximum of the SFs of the two LoRa signals is large enough. It also turns out that for the practical values of the SF, the squared magnitude of the cross-correlation in the discrete-time domain ranges between 0.04% and 1.08% of the peak value.
3) For some important special and asymptotic scenarios in both the continuous- and discrete-time domains, we further simplify the analytical expression of the cross-correlation and gain more insights.
4) In both the continuous- and discrete-time domains, we derive an asymptotically tight and analytically tractable upper bound of the cross-correlation. Also, we present the maximum strength of the cross-correlation for various practical values of the SF.
5) We present extensive numerical results that demonstrate the validity and accuracy of our analysis.

In Table I, our work and the related works in [6], [11], and [12] are compared in various aspects.

This article is organized as follows. In Section II, the LoRa signal model is described. In Sections III and IV, the quasi-orthogonality of the LoRa modulation is analyzed in the continuous- and discrete-time domains, respectively. Section V makes overall discussions and Section VI presents the numerical results. Finally, Section VII concludes this article.

*Notations:* The imaginary unit is denoted by $j \triangleq \sqrt{-1}$. Real and imaginary parts of a complex number $z$ are denoted by $\mathrm{Re}\{z\}$ and $\mathrm{Im}\{z\}$, respectively. $C(z) \triangleq \int_0^z \cos(\pi y^2/2)dy$ and $S(z) \triangleq \int_0^z \sin(\pi y^2/2)dy$ are Fresnel functions [15]. Also, $\mathcal{O}(f(z))$ and $o(f(z))$ denote big-O and little-o notations, respectively, which mean that $\lim_{z\to\infty}[\mathcal{O}(f(z))/f(z)] = c$ for some nonzero constant $c$ and $\lim_{z\to\infty}[o(f(z))/f(z)] = 0$. We use $(z)_{\mathrm{mod}\, y}$ to denote the remainder of the Euclidean division of $z$ by $y$, i.e., the modulo operation.

Also, all mathematical symbols used in this article are listed in Table II.

TABLE II
LIST OF MATHEMATICAL SYMBOLS USED IN THIS ARTICLE

| Mathematical symbol | Definition |
|---|---|
| $\mathrm{SF} \in \{7, 8, \cdots, 12\}$ | Spreading factor |
| $M = 2^{\mathrm{SF}}$ | Number of symbols in LoRa modulation under SF |
| $s \in \{0, 1, \cdots, M-1\}$ | Symbol of LoRa modulation under SF |
| $x(t)$ | Continuous-time LoRa signal |
| $B$ | Bandwidth |
| $T = \frac{M}{B}$ | Symbol duration of $x(t)$ |
| $t_\mathrm{f} = \frac{M-s}{B}$ | Folding time of $x(t)$ |
| $f_s$ | Sampling frequency |
| $x[n]$ | Discrete-time LoRa signal |
| $n_\mathrm{f} = t_\mathrm{f} f_s$ | Folding time of $x[n]$ sampled at $f_s$ |
| $x_1(t)$ and $x_2(t)$ | Two continuous-time LoRa signals |
| $\mathrm{SF}_1$ | Spreading factor of $x_1(t)$ (or $x_1[n]$) |
| $\mathrm{SF}_2$ ($< \mathrm{SF}_1$) | Spreading factor of $x_2(t)$ (or $x_2[n]$) |
| $M_1 = 2^{\mathrm{SF}_1}$ | Number of LoRa symbols for $x_1(t)$ (or $x_1[n]$) |
| $M_2 = 2^{\mathrm{SF}_2}$ ($< M_1$) | Number of LoRa symbols for $x_2(t)$ (or $x_2[n]$) |
| $T_1 = \frac{M_1}{B}$ | Symbol duration of $x_1(t)$ |
| $T_2 = \frac{M_2}{B}$ ($< T_1$) | Symbol duration of $x_2(t)$ |
| $\tau \in [0, T_1 - T_2]$ | Time delay of $x_2(t)$ |
| $s_1 \in \{0, 1, \cdots, M_1 - 1\}$ | LoRa symbol for $x_1(t)$ (or $x_1[n]$) |
| $s_2 \in \{0, 1, \cdots, M_2 - 1\}$ | LoRa symbol for $x_2(t)$ (or $x_2[n]$) |
| $t_i = \frac{M_i - s_i}{B}$, $i = 1, 2$ | Folding time of $x_i(t)$ |
| $\rho(\tau; s_1, s_2)$ | Cross-correlation between $x_1(t)$ and $x_2(t-\tau)$ |
| $\mathrm{Re}\{F(z, y)\}$ | $C(z+y) - C(z) = \int_z^y \cos\left(\frac{\pi x^2}{2}\right) dx$ |
| $\mathrm{Im}\{F(z, y)\}$ | $S(z+y) - S(z) = \int_z^y \sin\left(\frac{\pi x^2}{2}\right) dx$ |
| $\omega$, $\varphi$, and $\xi$ | Parameters contributing to the phase of $\rho(\tau; s_1, s_2)$ |
| $\alpha$, $\beta$, and $\gamma$ | Parameters contributing to the value of $\rho(\tau; s_1, s_2)$ |
| $\mu = \tau B$ | Parameter contributing to the values of $\omega$, $\varphi$, $\xi$, $\alpha$, and $\beta$ |
| $x_1[n]$ and $x_2[n]$ | Two discrete-time LoRa signals |
| $m \in \{0, 1, \cdots, M_1 - M_2\}$ | Time lag of $x_2[n]$ |
| $\varrho[m; s_1, s_2]$ | Cross-correlation between $x_1[n]$ and $x_2[n-m]$ |
| $\tilde{x}_i(t) = \sqrt{P_i} x_i(t)$, $i = 1, 2$ | Amplified version of $x_i(t)$ with gain $P_i$ |
| $\tilde{x}_i[n] = \sqrt{P_i} x_i[n]$, $i = 1, 2$ | Amplified version of $x_i[n]$ with gain $P_i$ |
| $\tilde{\rho}(\tau; s_1, s_2)$ | Cross-correlation between $\tilde{x}_1(t)$ and $\tilde{x}_2(t-\tau)$ |
| $\tilde{\varrho}[m; s_1, s_2]$ | Cross-correlation between $\tilde{x}_1[n]$ and $\tilde{x}_2[n-m]$ |

## II. LoRa SIGNAL MODEL

Let SF denote the SF (or the number of bits) that is a positive integer (which takes one value from $\{7, 8, \ldots, 12\}$ in practice [10]) and $M = 2^{\mathrm{SF}}$ be the number of symbols. Then, the continuous-time LoRa signal modulated with symbol $s \in \{0, 1, \ldots, M-1\}$ can be written as [3], [4], [5], and [6]

$$x(t) = \begin{cases} \exp\left(j2\pi\left[\left(\frac{s}{M} - \frac{1}{2}\right)Bt + \frac{B}{2T}t^2\right]\right), & 0 \le t < t_\mathrm{f} \\ \exp\left(j2\pi\left[\left(\frac{s}{M} - \frac{3}{2}\right)Bt + \frac{B}{2T}t^2\right]\right), & t_\mathrm{f} \le t < T \end{cases} \quad (1)$$

where $B$ denotes the bandwidth. Also, $T = (M/B)$ is the symbol (or chirp) duration and $t_f = (M - s/B)$ is the folding time.

The discrete-time representation of the LoRa modulated signal can be obtained by sampling the continuous-time waveform $x(t)$ at a sampling frequency $f_s$ (or equivalently, sampling interval $1/f_s$) as follows [3]:

$$x[n] \triangleq x\left(\frac{n}{f_s}\right) = \begin{cases} \exp\left(j2\pi\left[\left(\frac{s}{M} - \frac{1}{2}\right)\frac{B}{f_s}n + \frac{1}{2M}\left(\frac{B}{f_s}\right)^2 n^2\right]\right), & n \in \mathcal{N}_1 \\ \exp\left(j2\pi\left[\left(\frac{s}{M} - \frac{3}{2}\right)\frac{B}{f_s}n + \frac{1}{2M}\left(\frac{B}{f_s}\right)^2 n^2\right]\right), & n \in \mathcal{N}_2 \end{cases}$$

where $\mathcal{N}_1 = \{0, 1, \ldots, n_f - 1\}$ and $\mathcal{N}_2 = \{n_f, n_f + 1, \ldots, Tf_s - 1\}$. Also, $n_f = t_f f_s$. By setting $f_s = B$, it follows that [3], [4], [5], [6]:

$$x[n] = e^{j2\pi\left[\left(\frac{s}{M}-\frac{1}{2}\right)n+\frac{n^2}{2M}\right]}, \quad n = 0, 1, \ldots, M-1. \tag{2}$$

## III. Analysis on Quasi-Orthogonality of LoRa Modulation in Continuous-Time Domain

Consider two continuous-time LoRa signals, namely, $x_1(t)$ and $x_2(t)$, with different SFs, but occupying the same bandwidth $B$. Let $\mathrm{SF}_1$ and $\mathrm{SF}_2$ denote the SFs of $x_1(t)$ and $x_2(t)$, respectively. Without loss of generality, suppose that $\mathrm{SF}_1 > \mathrm{SF}_2$, and thus, $M_1 = 2^{\mathrm{SF}_1} > M_2 = 2^{\mathrm{SF}_2}$ and $T_1 = (M_1/B) > T_2 = (M_2/B)$. Also, $x_2(t)$ is assumed to involve an arbitrary time delay $\tau$ satisfying $0 \le \tau \le T_1 - T_2$.[1] Consequently, we have

$$x_1(t) = \begin{cases} e^{j2\pi\left[\left(\frac{s_1}{M_1}-\frac{1}{2}\right)Bt+\frac{B}{2T_1}t^2\right]}, & 0 \le t < t_1 \\ e^{j2\pi\left[\left(\frac{s_1}{M_1}-\frac{3}{2}\right)Bt+\frac{B}{2T_1}t^2\right]}, & t_1 \le t < T_1 \end{cases} \tag{3}$$

$$x_2(t-\tau) = \begin{cases} Ae^{j2\pi\left[\left(\frac{s_2}{M_2}-\frac{1}{2}\right)Bt+\frac{B}{2T_2}t^2\right]}, & \tau \le t < t_2 + \tau \\ \mathcal{A}e^{j2\pi\left[\left(\frac{s_2}{M_2}-\frac{3}{2}\right)Bt+\frac{B}{2T_2}t^2\right]}, & t_2 + \tau \le t < T_2 + \tau \\ 0, & \text{otherwise} \end{cases} \tag{4}$$

where $s_i$ is the modulation symbol of $x_i(t)$ and $t_i = ([M_i - s_i]/B)$ for $i = 1, 2$. Also

$$A = \exp\left(j2\pi\left[\frac{B}{2T_2}\tau^2 - \left(\frac{s_2}{M_2}-\frac{1}{2}\right)B\tau\right]\right) \tag{5}$$

$$\mathcal{A} = \exp\left(j2\pi\left[\frac{B}{2T_2}\tau^2 - \left(\frac{s_2}{M_2}-\frac{3}{2}\right)B\tau\right]\right). \tag{6}$$

[1]In this article, we focus on the analysis with $0 \le \tau \le T_1 - T_2$, even though our analysis and derived results can be readily extended to the case with $\tau > T_1 - T_2$, because we are interested in identifying the maximum strength of the cross-correlation. For the same reason, in the discrete-time domain, we focus on the analysis with a time lag $m \in \{0, 1, \ldots, M_1 - M_2\}$.

Note that the parameter $A$ in (5) [resp. $\mathcal{A}$ in (6)] represents a phase shift involved in $x_2(t-\tau)$ for $\tau \le t < t_2 + \tau$ (resp. for $t_2 + \tau \le t < T_2 + \tau$), which is induced by the time delay $\tau$. Interestingly, such as a phase shift is given in the form of a continuous-time up chirp with respect to $\tau$.

The cross-correlation between $x_1(t)$ and $x_2(t-\tau)$ (normalized to have the peak magnitude of unity) is defined as

$$\rho(\tau; s_1, s_2) \triangleq \frac{\int_0^{T_1} x_1^*(t)x_2(t-\tau)dt}{\sqrt{\int_0^{T_1}|x_1(t)|^2dt}\cdot\sqrt{\int_0^{T_1}|x_2(t-\tau)|^2dt}} = \sqrt{\frac{1}{T_1T_2}}\int_\tau^{\tau+T_2} x_1^*(t)x_2(t-\tau)dt. \tag{7}$$

To analyze the quasi-orthogonality of the LoRa modulation in the continuous-time domain, the cross-correlation $\rho(\tau; s_1, s_2)$ in (7) should be investigated. For this purpose, in the following, we derive a closed-form expression of $\rho(\tau; s_1, s_2)$ in terms of the Fresnel functions.

*Theorem 1:* For $0 \le \tau \le T_1 - T_2$, the cross-correlation between $x_1(t)$ and $x_2(t-\tau)$ is given by (8) (shown at the bottom of the page), where[2]

$$F(z, y) \triangleq \big(C(z+y) - C(z)\big) + j\big(S(z+y) - S(z)\big) \tag{9}$$

[2]Note that $F(z, y)$ defined in (9) denotes a complex exponential function involving the variants of Fresnel integrals in its real and imaginary parts such that

$$\mathrm{Re}\{F(z,y)\} = C(z+y) - C(z) = \int_z^y \cos\left(\frac{\pi x^2}{2}\right)dx$$

$$\mathrm{Im}\{F(z,y)\} = S(z+y) - S(z) = \int_z^y \sin\left(\frac{\pi x^2}{2}\right)dx.$$

Also, the other parameters in Theorem 1 are defined as follows. First, $\omega$, $\varphi$, and $\xi$ in (10)–(12) contribute to the phase of $\rho(\tau; s_1, s_2)$ in (8) for $0 \le \tau \le T_1 - T_2$, $0 \le \tau \le t_1 - t_2$, and $t_1 - t_2 < \tau \le T_1 - T_2$, respectively. Second, $\alpha$, $\beta$, and $\gamma$ in (13)–(15), respectively, contribute to the value of $\rho(\tau; s_1, s_2)$ in (8) by being used as the arguments of the function $F$. Third, $\mu = \tau B$ contributes to the values of $\omega$, $\varphi$, $\xi$, $\alpha$, and $\beta$.

$$\rho(\tau; s_1, s_2) = \begin{cases} \sqrt{\frac{1}{2(M_1-M_2)}}\left[Ae^{-j\omega}F\left(\alpha, \sqrt{\frac{2(M_1-M_2)}{M_1}} - \gamma\right) + \mathcal{A}e^{-j\varphi}F\left(\alpha - \sqrt{\frac{2M_1M_2}{M_1-M_2}} + \sqrt{\frac{2(M_1-M_2)}{M_1}} - \gamma, \gamma\right)\right], & \text{for } 0 \le \tau \le t_1 - T_2 \\ \sqrt{\frac{1}{2(M_1-M_2)}}\left[Ae^{-j\omega}F\left(\alpha, \sqrt{\frac{2(M_1-M_2)}{M_1}} - \gamma\right) + \mathcal{A}e^{-j\varphi}F\left(\alpha - \sqrt{\frac{2M_1M_2}{M_1-M_2}} + \sqrt{\frac{2(M_1-M_2)}{M_1}} - \gamma, \beta + \gamma - \sqrt{\frac{2(M_1-M_2)}{M_1}}\right) + \mathcal{A}e^{-j\omega}F\left(\beta, \alpha + \sqrt{\frac{2(M_1-M_2)}{M_1}} - \beta\right)\right], & \text{for } t_1 - T_2 < \tau \le t_1 - t_2 \\ \sqrt{\frac{1}{2(M_1-M_2)}}\left[Ae^{-j\omega}F(\alpha, \beta - \alpha) + Ae^{-j\xi}F\left(\beta + \sqrt{\frac{2M_1M_2}{M_1-M_2}}, \alpha + \sqrt{\frac{2(M_1-M_2)}{M_1}} - \beta - \gamma\right) + \mathcal{A}e^{-j\omega}F\left(\alpha + \sqrt{\frac{2(M_1-M_2)}{M_1}} - \gamma, \gamma\right)\right], & \text{for } t_1 - t_2 < \tau \le t_1 \\ \sqrt{\frac{1}{2(M_1-M_2)}}\left[Ae^{-j\xi}F\left(\alpha + \sqrt{\frac{2M_1M_2}{M_1-M_2}}, \sqrt{\frac{2(M_1-M_2)}{M_1}} - \gamma\right) + \mathcal{A}e^{-j\omega}F\left(\alpha + \sqrt{\frac{2(M_1-M_2)}{M_1}} - \gamma, \gamma\right)\right], & \text{for } t_1 < \tau \le T_1 - T_2. \end{cases} \tag{8}$$

$$\omega = \frac{\pi M_1 M_2}{M_1 - M_2}\left(\frac{s_2-\mu}{M_2} - \frac{s_1}{M_1}\right)^2 \quad (10)$$

$$\varphi = \frac{\pi M_1 M_2}{M_1 - M_2}\left(\frac{s_2-\mu}{M_2} - \frac{s_1}{M_1} - 1\right)^2 \quad (11)$$

$$\xi = \frac{\pi M_1 M_2}{M_1 - M_2}\left(\frac{s_2-\mu}{M_2} - \frac{s_1}{M_1} + 1\right)^2 \quad (12)$$

$$\alpha = \sqrt{\frac{2(M_1-M_2)}{M_1M_2}}\mu + \sqrt{\frac{2M_1M_2}{M_1-M_2}}\left(\frac{s_2-\mu}{M_2} - \frac{s_1}{M_1}\right) \quad (13)$$

$$\beta = \sqrt{\frac{2(M_1-M_2)}{M_1M_2}}(M_1 - s_1) + \sqrt{\frac{2M_1M_2}{M_1-M_2}}\left(\frac{s_2-\mu}{M_2} - \frac{s_1}{M_1}\right) \quad (14)$$

$$\gamma = \sqrt{\frac{2(M_1-M_2)}{M_1M_2}}s_2. \quad (15)$$

In (10)–(14), $\mu = \tau B$.

*Proof:* See Appendix A-A. ■

From Theorem 1, it turns out that the cross-correlation between $x_1(t)$ and $x_2(t-\tau)$ is inversely proportional to the difference between the amounts of symbols of the two LoRa signals (i.e., $M_1 - M_2$). Also, the cross-correlation relies on the time delay $\tau$ as well as the symbols and SFs of the two LoRa signals (i.e., the set of parameters $\{\tau, s_1, s_2, \mathrm{SF}_1, \mathrm{SF}_2\}$); but, it is irrelevant of the bandwidth $B$.[3]

In the following, we further investigate some important special and asymptotic cases where the expression of the cross-correlation becomes much simplified.

1) *Cross-Correlation for Special Case:* First, for a special case when $\tau = s_1 = s_2 = 0$,[4] the cross-correlation is presented in the following.

*Corollary 1:* The cross-correlation between $x_1(t)$ and $x_2(t)$ with $s_1 = s_2 = 0$ is given by

$$\rho(0;0,0) = \sqrt{\frac{1}{2(M_1-M_2)}}\left[C\left(\sqrt{\frac{2M_2(M_1-M_2)}{M_1}}\right) + jS\left(\sqrt{\frac{2M_2(M_1-M_2)}{M_1}}\right)\right]. \quad (16)$$

*Proof:* When $\tau = s_1 = s_2 = 0$, we have $\omega = \varphi = \xi = \alpha = \gamma = \mu = 0$, and $t_i = T_i$, $i = 1, 2$. By substituting these into (8) and using the fact that $C(0) = S(0) = 0$ [15], the result of (16) can be obtained. ■

2) *Cross-Correlation for Asymptotic Cases:* For asymptotic analysis, we again consider the case of $\tau = s_1 = s_2 = 0$. In what follows, we derive the cross-correlation for two asymptotic cases.

*Corollary 2:* For fixed $(M_1/M_2) < \infty$, when $M_2 \to \infty$, the cross-correlation between $x_1(t)$ and $x_2(t)$ with $s_1 = s_2 = 0$ approaches

$$\rho(0;0,0) \to \sqrt{\frac{1}{2(M_1-M_2)}}\left\{\left[\frac{1}{2} + \frac{1}{\pi}\sqrt{\frac{M_1}{2M_2(M_1-M_2)}}\sin\left(\frac{\pi M_2(M_1-M_2)}{M_1}\right)\right] + j\left[\frac{1}{2} - \frac{1}{\pi}\sqrt{\frac{M_1}{2M_2(M_1-M_2)}}\cos\left(\frac{\pi M_2(M_1-M_2)}{M_1}\right)\right]\right\}. \quad (17)$$

*Proof:* By using the Taylor expansion, it can be shown that $C(z) \approx (1/2) + (1/\pi z)\sin(\pi z^2/2)$ and $S(z) \approx (1/2) - (1/\pi z)\cos(\pi z^2/2)$ for $z \gg 1$. By applying these expansions to (16), the result of (17) can be obtained. ■

The result of Corollary 2 implies that for the case when $M_1$ is asymptotically large with fixed $(M_1/M_2)$, the value of $\rho(0;0,0)$ can be computed very efficiently because the integration involved in the Fresnel functions does not need to be computed.

The results of Corollaries 1 and 2 still show that the cross-correlation is inversely proportional to $M_1 - M_2$ even when $\tau = s_1 = s_2 = 0$. On the other hand, interestingly, there is an exceptional case where the cross-correlation is inversely proportional only to $M_1$, which is shown in the following.

*Corollary 3:* For fixed $M_2 < \infty$, when $M_1 \to \infty$, the cross-correlation between $x_1(t)$ and $x_2(t)$ with $s_1 = s_2 = 0$ approaches

$$\rho(0;0,0) \to \sqrt{\frac{1}{2M_1}}\left[C\left(\sqrt{2M_2}\right) + jS\left(\sqrt{2M_2}\right)\right]. \quad (18)$$

*Proof:* When $M_1 \to \infty$ with fixed $M_2 < \infty$, it follows that $M_1 - M_2 \to M_1$. Substituting this into (16), the result of (18) can be obtained. ■

The remaining important question is whether the LoRa modulation is indeed quasi-orthogonal in the continuous-time domain. The answer turns out to be affirmative if one of the SFs of the two LoRa signals is large enough. For more detailed analysis and discussions, in the following, we derive a tight upper bound of the strength of the cross-correlation between $x_1(t)$ and $x_2(t-\tau)$.

*Theorem 2:* $|\rho(\tau; s_1, s_2)|^2$ is upper bounded by

$$\left|\rho(\tau; s_1, s_2)\right|^2 \lesssim \frac{1.677}{M_1 - M_2}. \quad (19)$$

*Proof:* See Appendix A-B. ■

From Theorem 2, it turns out that the squared magnitude (or power) of the cross-correlation between $x_1(t)$ and $x_2(t-\tau)$ is of the order of

$$\left|\rho(\tau; s_1, s_2)\right|^2 = \mathcal{O}\left(\frac{1}{M_1 - M_2}\right) \quad (20)$$

which is inversely proportional to $M_1 - M_2$. That is, the larger the value of $M_1 - M_2$ is, the smaller the strength of the cross-correlation is in the continuous-time domain. This is the case when either $\mathrm{SF}_1$ or $\mathrm{SF}_2$ is large since $M_1 - M_2$ is large when $M_1$ is large for fixed $M_2$ or when $M_2$ is large for fixed $(M_1/M_2)$. Therefore, the results of (19) and (20) imply that the two nonsynchronized LoRa signals modulated under different SFs are quasi-orthogonal in the continuous-time domain when one of the SFs of the two LoRa signals is large enough.

[3]Note, however, that as shown in (37), the *unnormalized* cross-correlation (i.e., inner product) between $x_1(t)$ and $x_2(t)$ depends on the bandwidth $B$.

[4]In practice, this case corresponds to the transmission of two synchronized preamble signals (i.e., basic up chirps) modulated under different SFs.

## IV. Analysis on Quasi-Orthogonality of LoRa Modulation in Discrete-Time Domain

For analysis, let us consider two discrete-time LoRa signals, namely, $x_1[n]$ and $x_2[n]$, with different SFs, i.e., $\mathrm{SF}_1$ and $\mathrm{SF}_2$, respectively. Also, $x_2[n]$ involves an arbitrary time lag $m$ satisfying $m \in \{0, 1, \ldots, M_1 - M_2\}$. Thus, we have

$$x_1[n] = e^{j2\pi\left[\left(\frac{s_1}{M_1}-\frac{1}{2}\right)n+\frac{n^2}{2M_1}\right]},\quad n = 0, 1, \ldots, M_1 - 1, \tag{21}$$

$$x_2[n-m] = \begin{cases} \Lambda e^{j2\pi\left[\left(\frac{s_2-m}{M_2}-\frac{1}{2}\right)n+\frac{n^2}{2M_2}\right]}, & n = m, \ldots, M_2 + m - 1 \\ 0, & \text{otherwise} \end{cases} \tag{22}$$

where

$$\Lambda = \exp\left(j2\pi\left[\frac{m^2}{2M_2} - \left(\frac{s_2}{M_2} - \frac{1}{2}\right)m\right]\right) \tag{23}$$

which represents a phase shift involved in $x_2[n-m]$, being induced by the time lag $m$.

The cross-correlation between $x_1[n]$ and $x_2[n-m]$ is defined as

$$\begin{aligned}\varrho[m; s_1, s_2] &\triangleq \frac{\sum_{n=0}^{M_1-1} x_1^*[n]x_2[n-m]}{\sqrt{\sum_{n=0}^{M_1-1}|x_1[n]|^2}\cdot\sqrt{\sum_{n=0}^{M_1-1}|x_2[n-m]|^2}} \\ &= \sqrt{\frac{1}{M_1M_2}}\sum_{n=m}^{M_2+m-1} x_1^*[n]x_2[n-m].\end{aligned} \tag{24}$$

In the following, we derive a useful expression of $\varrho[m; s_1, s_2]$ in an exponential form.

*Theorem 3:* For $m \in \{0, 1, \ldots, M_1 - M_2\}$, the cross-correlation between $x_1[n]$ and $x_2[n-m]$ takes the following form:

$$\varrho[m; s_1, s_2] = \sqrt{\frac{1}{M_1M_2}}\Lambda r \exp(j\theta) \tag{25}$$

where

$$r = \sqrt{M_2 + 2\sum_{n=0}^{M_2-1}\sum_{l=0}^{n-1}\cos\left(2\pi(l-n)[a(l+n+2m)+b]\right)} \tag{26}$$

$$\theta = \tan^{-1}\left(\frac{\sum_{n=0}^{M_2-1}\sin\left(2\pi\left[a(n+m)^2+b(n+m)\right]\right)}{\sum_{n=0}^{M_2-1}\cos\left(2\pi\left[a(n+m)^2+b(n+m)\right]\right)}\right). \tag{27}$$

In (26) and (27), $a = (1/2)([1/M_2] - [1/M_2])$ and $b = ([s_2 - m]/M_2) - (s_1/M_1)$.

*Proof:* See Appendix A-C. ■

In what follows, several special and asymptotic cases are investigated, in which the expression of the cross-correlation becomes further simplified and useful insights are obtained.

1) *Cross-Correlation for Some Special Cases:* First, we have the following result.

*Theorem 4:* For $M_1 = 2M_2$, when $M_1s_2 - M_2s_1$ is a multiple of $M_1$ and $m$ is an even number, the cross-correlation between $x_1[n]$ and $x_2[n-m]$ is given by (28) (shown at the bottom of this page), where $i = (s_2 - m - [M_2/M_1]s_1)_{\mathrm{mod}M_2}$ and $k = i + (m/2)_{\mathrm{mod}M_2}$.

*Proof:* See Appendix A-D. ■

Note that when $s_1 = s_2 = 0$, $M_1s_2 - M_2s_1$ is always a multiple of $M_1$. The cross-correlation in this case with $m = 0$ is presented in the following.

*Corollary 4:* When $M_1 = 2M_2$, the cross-correlation between $x_1[n]$ and $x_2[n]$ with $m = s_1 = s_2 = 0$ is given by

$$\varrho[0; 0, 0] = \sqrt{\frac{1}{2M_1}}\exp\left(j\frac{\pi}{4}\right) \tag{29}$$

*Proof:* When $m = s_1 = s_2 = 0$, we have $i = k = 0$ in (28). By substituting this into (28), the result of (29) can be obtained. ■

Intriguingly, from Corollary 4, it turns out that when $m = s_1 = s_2 = 0$, the cross-correlation between the two discrete-time LoRa signals is inversely proportional to the maximum number of symbols between the two LoRa signals (i.e., $M_1$), or equivalently, the maximum of the SFs of the two LoRa signals (i.e., $\mathrm{SF}_1$), with a constant phase of $(\pi/4)$.

2) *Cross-Correlation for Asymptotic Cases:* For asymptotic cases, we have the following results.

*Theorem 5:* For fixed $M_2 < \infty$, when $M_1 \to \infty$ and $M_1s_2 - M_2s_1$ is a multiple of $M_1$, the cross-correlation between $x_1[n]$ and $x_2[n-m]$ with $m = o(M_1)$ approaches

$$\varrho[m; s_1, s_2] \to \sqrt{\frac{1}{M_1}}\exp\left[j\pi\left(\frac{1}{4} - \frac{k^2}{M_2}\right)\right] \tag{30}$$

where $k = (s_2 - m - [M_2/M_1]s_1)_{\mathrm{mod}M_2}$.

*Proof:* See Appendix A-E. ■

When $m = s_1 = s_2 = 0$, the result of Theorem 5 is simplified as follows:

*Corollary 5:* For fixed $M_2 < \infty$, when $M_1 \to \infty$, the cross-correlation between $x_1[n]$ and $x_2[n]$ with $s_1 = s_2 = 0$ approaches

$$\varrho[0; 0, 0] \to \sqrt{\frac{1}{M_1}}\exp\left(j\frac{\pi}{4}\right). \tag{31}$$

*Proof:* When $m = s_1 = s_2 = 0$, we have $k = 0$ in (30). From this, the result of (31) can be obtained. ■

From Theorem 5 and Corollary 5, it turns out that even for the case of the asymptotically large $M_1$ with fixed $M_2$, the cross-correlation is again inversely proportional to $M_1$.

$$\varrho[m; s_1, s_2] = \begin{cases} \sqrt{\frac{1}{2M_1}}\Lambda\exp\left[j\pi\left(\frac{1}{4} + \frac{2m(i+m/4)}{M_2}\right)\right], & k = 0 \\ \sqrt{\frac{1}{2M_1}}\Lambda\left\{\exp\left[j\pi\left(\frac{1}{4} - \frac{2\left[k^2 - m(i+m/4)\right]}{M_2}\right)\right]\right. \\ \quad \left. -2\sqrt{\frac{2}{M_1M_2}}\exp\left(-j\pi\frac{2k^2 - m(2i+m/2) - 1/2}{M_2}\right)\sum_{l=0}^{k-1}\exp\left(j2\pi\frac{l(l+1)}{M_2}\right)\right\}, & \text{otherwise.} \end{cases} \tag{28}$$

An important observation from the above results is that the LoRa modulation is quasi-orthogonal in the discrete-time domain if the maximum of the SFs of the two LoRa signals is large enough. For more detailed analysis and discussions, we present the following result.

*Theorem 6:* $|\varrho[m; s_1, s_2]|^2$ is upper bounded by

$$\left|\varrho[m; s_1, s_2]\right|^2 \leq \frac{1+2\varepsilon}{M_1} \tag{32}$$

where

$$\varepsilon = \max_{s_1, s_2, m, n} \sum_{l=0}^{n-1} \cos\left(2\pi(l-n)[a(l+n+2m)+b]\right). \tag{33}$$

*Proof:* See Appendix A-F. ■

From Theorem 6, it turns out that the squared magnitude of the cross-correlation between $x_1[n]$ and $x_2[n-m]$ is of the order of

$$\left|\varrho[m; s_1, s_2]\right|^2 = \mathcal{O}\left(\frac{1}{M_1}\right) \tag{34}$$

which is inversely proportional to $M_1$, or equivalently, $\mathrm{SF}_1$ (i.e., the maximum of the SFs of the two LoRa signals). This implies that the two nonsynchronized LoRa signals modulated under different SFs are quasi-orthogonal in the discrete-time domain when the maximum SF value is large enough.

## V. Overall Discussions

In this section, we make overall discussions on the quasi-orthogonality of the LoRa modulation, and we provide practically useful and theoretically unified insights. For this purpose, in the following, we first present the asymptotic quasi-orthogonality of the LoRa modulation.

*Theorem 7:* When $M_1 \to \infty$ with fixed $M_2 < \infty$ or when $M_2 \to \infty$ with fixed $(M_1/M_2) < \infty$, it follows that:

$$\left|\rho(\tau; s_1, s_2)\right|^2 \to 0 \quad \text{and} \quad \left|\varrho[m; s_1, s_2]\right|^2 \to 0. \tag{35}$$

*Proof:* See Appendix A-G. ■

Based on Theorem 7 along with the theoretical results derived in the previous sections, we can make the following conclusions.

1) The quasi-orthogonality of the LoRa modulation is guaranteed in both the continuous- and discrete-time domains for large $M_1$ and/or $M_2$ (and thus, when either $\mathrm{SF}_1$ or $\mathrm{SF}_2$ is large). Quite surprisingly, this also means that if the SF values are small, the quasi-orthogonality may not be ensured, possibly resulting in unwanted crosstalk between the LoRa signals in practice. To address this issue, one should carefully select the SFs of the LoRa signals according to the required crosstalk levels. An intuitive way is to choose the value of $\mathrm{SF}_1$ as large as possible by selecting the value of $\mathrm{SF}_2$ as small as possible or keeping the value of $\mathrm{SF}_2$ constant.
2) From Theorem 7, it can be also inferred that the two nonsynchronized LoRa signals are quasi-orthogonal in both the continuous- and discrete-time domains if they are quasi-orthogonal in at least one of the two domains.

Next, we further investigate the unnormalized cross-correlation (i.e., inner product) of the LoRa modulation, additionally taking the amplification gains of the LoRa signals into account. Specifically, let

$$\tilde{x}_i(t) = \sqrt{P_i}x_i(t) \text{ and } \tilde{x}_i[n] = \sqrt{P_i}x_i[n], \quad i = 1, 2 \tag{36}$$

where $\sqrt{P_i}$ denotes the amplification gain, which accounts for the amplifier effects, transmit power, fading channel gain, distortion, etc. Then the inner product between $\tilde{x}_1(t)$ and $\tilde{x}_2(t-\tau)$ and that between $\tilde{x}_1[n]$ and $\tilde{x}_2[n-m]$ are, respectively, given by

$$\begin{aligned}\tilde{\rho}(\tau; s_1, s_2) &= \int_{\tau}^{\tau+T_2} \tilde{x}_1^*(t)\tilde{x}_2(t-\tau)dt \\ &\propto \frac{\sqrt{P_1 P_2}}{B}\rho(\tau; s_1, s_2) \end{aligned} \tag{37}$$

$$\begin{aligned}\tilde{\varrho}[m; s_1, s_2] &= \sum_{n=m}^{M_2+m-1} \tilde{x}_1^*[n]\, \tilde{x}_2[n-m] \\ &= \sqrt{P_1 P_2}\varrho[m; s_1, s_2].\end{aligned} \tag{38}$$

From (37) and (38), it turns out that in both continuous- and discrete-time domains, the inner product is proportional to the amplification gains of the LoRa signals. In the continuous-time domain, it is also inversely proportional to the bandwidth. Therefore, in practice, there are several additional situations where the quasi-orthogonality may not be guaranteed. Specifically, if the amplification gain of the crosstalk signal is large and/or the bandwidth of the system is small, the quasi-orthogonality of the LoRa modulation might not be established. Thus, to achieve the quasi-orthogonality, one should maximize the bandwidth and at the same time minimize the amplification gain of the crosstalk signal as well.

Finally, we provide more discussions on how the analytical results derived in this article can be used for the practical LoRa system designs. First of all, for the cases of the LoRa system designs dealing only with the crosstalk (or interference) issue, our analysis gives us the following fundamental, yet important and valuable, insights.

1) If the LoRa systems operate in the continuous-time domain, the SF values should be maximized as much as possible to minimize the impact of the crosstalk between the continuous-time LoRa signals with different SFs.[5]
2) On the other hand, if the LoRa systems operate in the discrete-time domain, the maximum SF value should be maximized as much as possible to minimize the impact of the crosstalk between the discrete-time LoRa signals with different SFs.

In addition, the derived analytical results can be used for the practical LoRa system designs in terms of resource allocation (e.g., SF allocation or power allocation) by performing optimizations with various design criteria (such as bit error rate (BER), data rate, coverage, etc.) under the constraint on the crosstalk as follows.

1) For example, suppose that one is interested in the LoRa system designs for the SF allocation with BER minimization (or coverage maximization). Let

[5]However, a large SF value results in increasing the symbol duration, thus, increasing the probability of collision. In practice, therefore, one should judiciously select the SF value according to the required collision tolerance as well.

$\mathcal{E}(\mathrm{SF}_1, \mathrm{SF}_2)$ denote a performance measure (such as average BER, maximum BER, etc.) for the BERs of the two LoRa signals with different SFs (i.e., $x_1(t)$ and $x_2(t)$ in the continuous-time domain or $x_1[n]$ and $x_2[n]$ in the discrete-time domain), which is a function of $\mathrm{SF}_1$ and $\mathrm{SF}_2$. Also, let $\mathcal{S}$ denote a set of SF values satisfying the crosstalk constraint, which is defined as[6]

$$\mathcal{S} = \begin{cases} \left\{(\mathrm{SF}_1, \mathrm{SF}_2) : \max\limits_{\tau, s_1, s_2} \left|\rho(\tau; s_1, s_2)\right| \le \rho_{\mathrm{th}}\right\} \\ \qquad \text{in the continuous-time domain} \\ \left\{(\mathrm{SF}_1, \mathrm{SF}_2) : \max\limits_{m, s_1, s_2} \left|\varrho[m; s_1, s_2]\right| \le \varrho_{\mathrm{th}}\right\} \\ \qquad \text{in the discrete -time domain} \end{cases} \tag{39}$$

where $\rho_{\mathrm{th}}$ or $\varrho_{\mathrm{th}}$ denotes a threshold for the maximum cross-correlation strength. Then, the SF allocation for the BER minimization can be done via

$$\underset{(\mathrm{SF}_1, \mathrm{SF}_2) \in \mathcal{S}}{\text{minimize}} \quad \mathcal{E}(\mathrm{SF}_1, \mathrm{SF}_2). \tag{40}$$

2) Similarly, for the LoRa system designs with the aim of data rate maximization, the SF allocation can be conducted by

$$\underset{(\mathrm{SF}_1, \mathrm{SF}_2) \in \mathcal{S}}{\text{maximize}} \quad \mathcal{R}(\mathrm{SF}_1, \mathrm{SF}_2) \tag{41}$$

where $\mathcal{R}(\mathrm{SF}_1, \mathrm{SF}_2)$ denotes a performance measure (such as sum rate, minimum rate, etc.) for the data rates of the two LoRa signals with different SFs as a function of $\mathrm{SF}_1$ and $\mathrm{SF}_2$.

## VI. Numerical Results

In this section, numerical results are presented to validate our analysis in the previous sections. Since LoRa supports six different values for the SF (from 7 to 12) in practice, we set $\mathrm{SF}_i \in \{7, 8, \dots, 12\}$, $i = 1, 2$, in the simulations (unless specified otherwise).

In Fig. 1, the cross-correlation between $x_1(t)$ and $x_2(t - \tau)$ is shown versus the time delay $\tau$ when $s_1 = s_2 = 0$, $\mathrm{SF}_1 = 12$, and $\mathrm{SF}_2 \in \{8, 11\}$. It can be observed from Fig. 1 that the strength of the cross-correlation tends to decrease as $\tau$ increases, while its phase is arbitrarily and almost uniformly distributed across $[-\pi, \pi)$. Fig. 2 depicts the cross-correlation between $x_1(t)$ and $x_2(t)$ versus the symbol $s_1$ of $x_1(t)$ when $s_2 = 0$, $\mathrm{SF}_1 = 12$, and $\mathrm{SF}_2 = 11$. From Fig. 2, it can be inferred that there exist certain fairs of the LoRa symbols that make the strength of the cross-correlation large or small.

In Figs. 3 and 4, the cross-correlation between $x_1(t)$ and $x_2(t)$ is plotted versus $\mathrm{SF}_2$ when $\mathrm{SF}_1 = 12$ and $\mathrm{SF}_1$ when $\mathrm{SF}_2 = 7$, respectively, where $s_1 = s_2 = 0$. From Figs. 3 and 4, we can observe that the strength of the cross-correlation decreases as $\mathrm{SF}_2$ decreases for fixed $\mathrm{SF}_1$ or $\mathrm{SF}_1$ increases for fixed $\mathrm{SF}_2$, as expected from our analysis in Section III. Also,

[6]Note that in (39), the expression of $\rho(\tau; s_1, s_2)$ in the continuous-time domain (resp. $\varrho[m; s_1, s_2]$ in the discrete-time domain) can take one of those in (8) and (16)–(19) [resp. (25) and (28)–(32)] depending on the operating condition of the LoRa system.

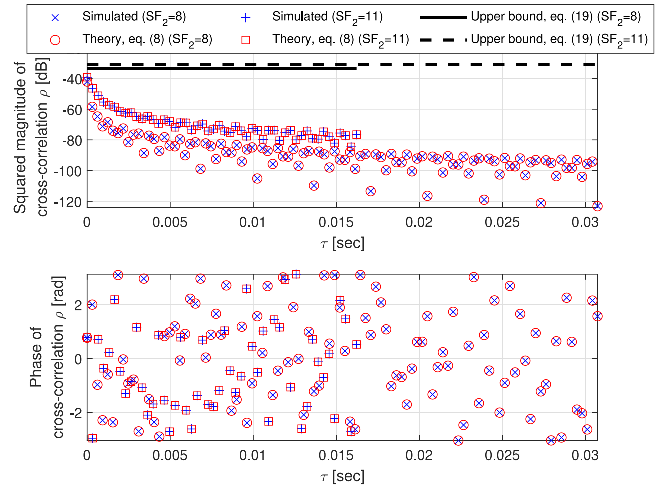


Fig. 1. $\rho(\tau; 0, 0)$ versus $\tau$ when $\mathrm{SF}_1 = 12$ and $\mathrm{SF}_2 \in \{8, 11\}$.

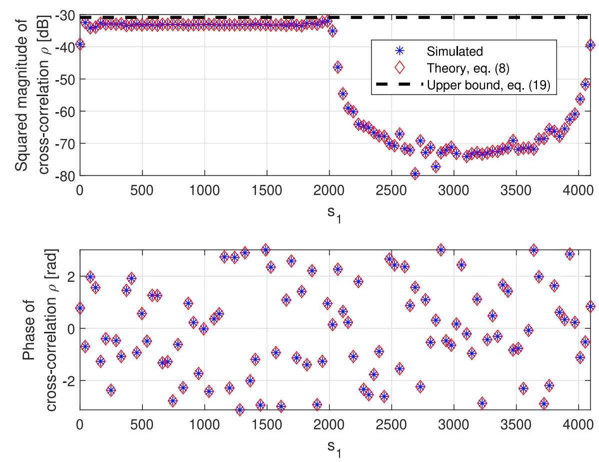


Fig. 2. $\rho(0; s_1, 0)$ versus $s_1$ when $\mathrm{SF}_1 = 12$ and $\mathrm{SF}_2 = 11$.

the asymptotic analysis presented in Section III-2) agrees well for large $\mathrm{SF}_1$ or $\mathrm{SF}_2$.

In Table III, the maximum value of $|\rho(\tau; s_1, s_2)|^2$ obtained based on (8) is presented for various practical values of the SF (i.e., $7, 8, \dots, 12$) together with the corresponding upper bound given by (19), of which value is shown in bracket. From Table III, it can be observed that for the practical values of the SF, the squared magnitude of the cross-correlation ranges between 0.04% and 1.14% of the peak value (i.e., unity). It is small when $\mathrm{SF}_1$ or $\mathrm{SF}_2$ is large, which accords with our analysis. Also, given $\mathrm{SF}_1$ (resp. $\mathrm{SF}_2$), the strength of the cross-correlation tends to be smaller when $\mathrm{SF}_2$ becomes smaller (resp. when $\mathrm{SF}_1$ becomes larger), because $M_1 - M_2$ gets larger.

Fig. 5 shows the cross-correlation between $x_1[n]$ and $x_2[n - m]$ as a function of the time lag $m$ when $s_1 = (M_1/M_2)$, $s_2 = M_2 - 1$, $\mathrm{SF}_1 = 10$, and $\mathrm{SF}_2 = 9$, where $m$ is set to be even numbers. From Fig. 5, it can be seen that the strength of the cross-correlation is not monotonic over $m$, unlike the case in the continuous-time domain. The cross-correlation is observed to be strong when $m$ is very small or very large. In Fig. 6, we plot the cross-correlation between $x_1[n]$ and $x_2[n - m]$ as a function of the symbol $s_2$ of $x_2[n - m]$ when $m = s_1 = 0$,

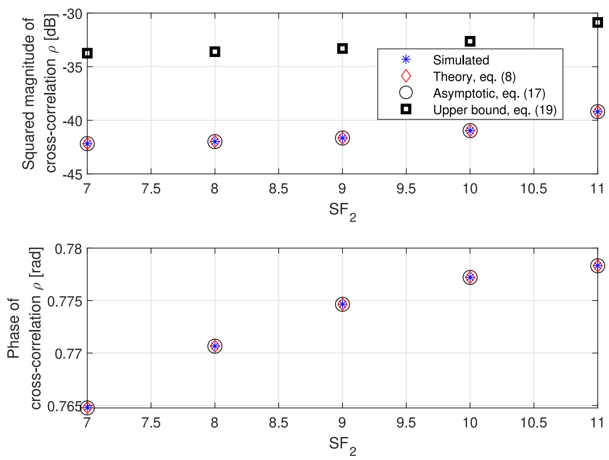


Fig. 3. $\rho(0; 0, 0)$ versus $\mathrm{SF}_2$ when $\mathrm{SF}_1 = 12$.

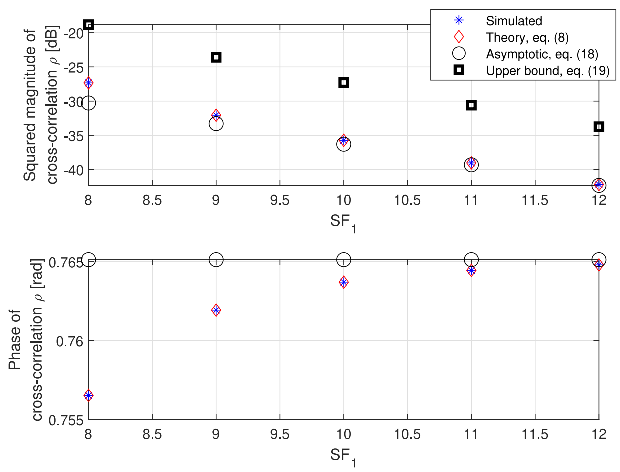


Fig. 4. $\rho(0; 0, 0)$ versus $\mathrm{SF}_1$ when $\mathrm{SF}_2 = 7$.

TABLE III
MAXIMUM VALUE AND UPPER BOUND OF SQUARED MAGNITUDE OF CROSS-CORRELATION BETWEEN CONTINUOUS-TIME LORA SIGNALS

| | | $\mathrm{SF}_1$ | | | | |
|---|---|---|---|---|---|---|
| | | 12 | 11 | 10 | 9 | 8 |
| $\mathrm{SF}_2$ | 7 | 0.0004 (0.0004) | 0.0007 (0.0009) | 0.0016 (0.0019) | 0.0038 (0.0044) | 0.0114 (0.0131) |
| | 8 | 0.0004 (0.0004) | 0.0008 (0.0009) | 0.0018 (0.0022) | 0.0055 (0.0066) | |
| | 9 | 0.0004 (0.0005) | 0.0009 (0.0011) | 0.0027 (0.0033) | | |
| | 10 | 0.0005 (0.0005) | 0.0014 (0.0016) | | | |
| | 11 | 0.0007 (0.0008) | | | | |

*The value in the bracket denotes the upper bound in (19).

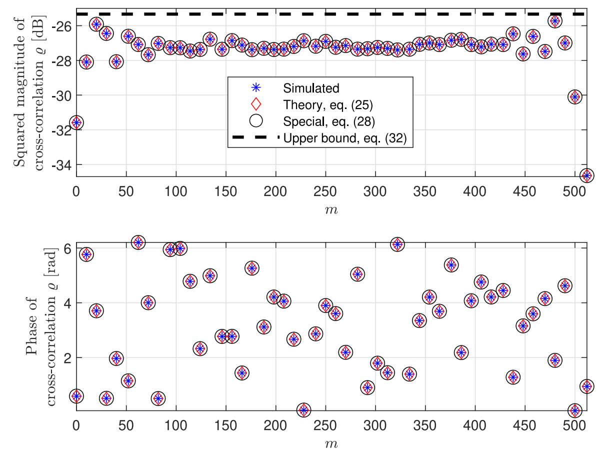


Fig. 5. $\varrho[m; (M_1/M_2), M_2-1]$ versus even $m$ when $\mathrm{SF}_1 = 10$ and $\mathrm{SF}_2 = 9$.

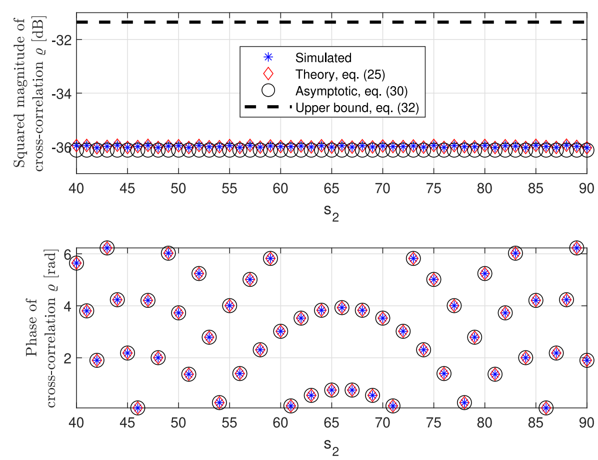


Fig. 6. $\varrho[0; 0, s_2]$ versus $s_2$ when $\mathrm{SF}_1 = 12$ and $\mathrm{SF}_2 = 7$.

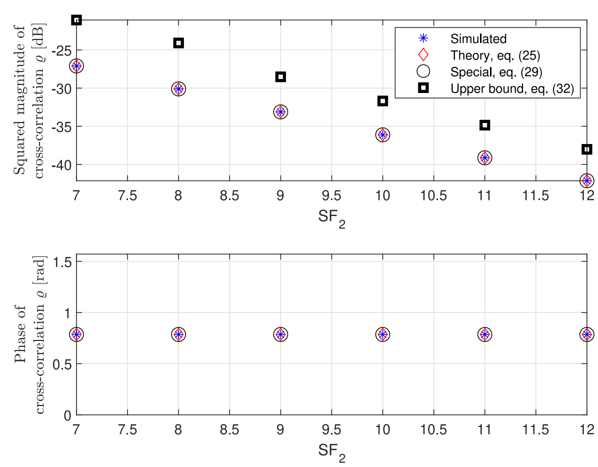


Fig. 7. $\varrho[0; 0, 0]$ versus $\mathrm{SF}_2$ when $\mathrm{SF}_1 = 2\mathrm{SF}_2$.

$\mathrm{SF}_1 = 12$, and $\mathrm{SF}_2 = 7$. Also, in Figs. 7 and 8, the cross-correlation between $x_1[n]$ and $x_2[n]$ is shown versus $\mathrm{SF}_2$ when $\mathrm{SF}_1 = 2\mathrm{SF}_2$ and versus $\mathrm{SF}_1$ when $\mathrm{SF}_2 = 7$, respectively. We set $m = s_1 = s_2 = 0$ in Fig. 7 and $m = 0$, $s_1 = (M_1/M_2)$, and $s_2 = M_2 - 1$ in Fig. 8. From Figs. 6 and 8, one can see the results expected from Theorem 5 and Corollary 5, respectively. Also, from Fig. 7, one can see that as $\mathrm{SF}_1$ increases, the cross-correlation tends to have a monotonically decreasing strength over $\mathrm{SF}_1$ with the constant phase of $(\pi/4)$, which accords with the result of Corollary 4.

Table IV lists the maximum value of $|\varrho[m; s_1, s_2]|^2$ obtained based on (25) for the practical values of the SF along with the corresponding upper bound in (19), of which value is shown in the bracket. From Table IV, it can be observed that for the practical values of the SF, the squared magnitude of the cross-correlation in the discrete-time domain ranges between 0.04% and 1.08% of the peak value (i.e., unity). It is small

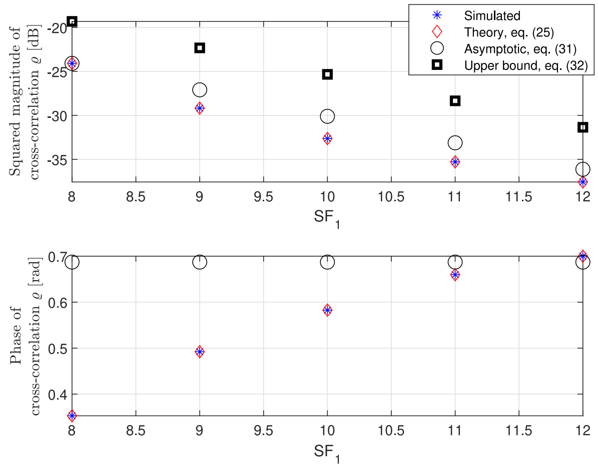


Fig. 8. $\varrho[0; (M_1/M_2), M_2 - 1]$ versus $\mathrm{SF}_1$ when $\mathrm{SF}_2 = 7$.

TABLE IV
MAXIMUM VALUE AND UPPER BOUND OF SQUARED MAGNITUDE OF CROSS-CORRELATION BETWEEN DISCRETE-TIME LORA SIGNALS

| | | $\mathrm{SF}_1$ | | | | |
|---|---|---|---|---|---|---|
| | | 12 | 11 | 10 | 9 | 8 |
| $\mathrm{SF}_2$ | 7 | 0.0004 (0.0007) | 0.0008 (0.0015) | 0.0017 (0.0029) | 0.0038 (0.0059) | 0.0108 (0.0117) |
| | 8 | 0.0004 (0.0007) | 0.0008 (0.0015) | 0.0019 (0.0029) | 0.0054 (0.0059) | |
| | 9 | 0.0004 (0.0007) | 0.0009 (0.0015) | 0.0027 (0.0029) | | |
| | 10 | 0.0004 (0.0007) | 0.0013 (0.0015) | | | |
| | 11 | 0.0007 (0.0007) | | | | |

*The value in the bracket denotes the upper bound in (32).

when $\mathrm{SF}_1$ is large, which accords with our analysis. Also, given the same $\mathrm{SF}_1$, the strength of the cross-correlation tends to be smaller when $\mathrm{SF}_2$ gets smaller. Thus, a large SF gap is even beneficial for ensuring the quasi-orthogonality in the discrete-time domain.

Finally, from the results in Figs. 1–4 and Table III, it can be concluded that the upper bound derived in (19) is highly accurate when the magnitude of the cross-correlation is large (even otherwise, it still results in a sufficiently small error). In this sense, therefore, the upper bound in (19) can be considered to be (almost) tight. A similar conclusion can be made for the upper bound derived in (32) based on the results in Figs. 5–8 and Table III. Thus, the upper bound in (32) can be considered to be (almost) tight as well.

## VII. CONCLUSION

In this article, we investigated and analyzed the quasi-orthogonality of the LoRa modulation by deriving the cross-correlation between the two nonsynchronized LoRa signals with different SFs in both continuous- and discrete-time domains. It was analytically shown that in the continuous-time domain, the quasi-orthogonality is guaranteed when one of SFs of the two LoRa signals is large enough; while, in the discrete-time domain, the quasi-orthogonality is ensured when the maximum of the SFs is large enough. From the derived results, we also provided the useful engineering insights and further discussed on the quasi-orthogonality of the LoRa modulation in depth. The validity and accuracy of our analysis were demonstrated via the numerical results.

As an intriguing and important focus of future research, it is deserved to study performance analysis, SF allocation, superposition coding, frequency/time synchronization, and so on when multiple LoRa users employing different SFs coexist and interfere with each other, based on the results presented in this article.

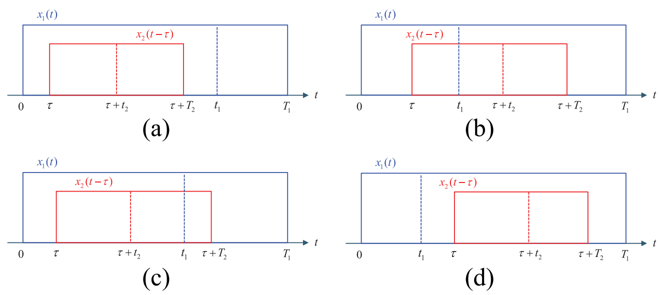


Fig. 9. Illustrative example for the four difference cases analyzed in Theorem 1, which are differ in how $x_1(t)$ and $x_2(t-\tau)$ are cross-correlated depending on the duration of their folding times $t_1$ and $t_2+\tau$ as well as the time delay $\tau$. (a) When $0 \le \tau \le t_1 - T_2$. (b) When $t_1 - T_2 < \tau \le t_1 - t_2$. (c) When $t_1 - t_2 < \tau \le t_1$. (d) When $t_1 < \tau \le T_1 - T_2$.

## APPENDIX A
## PROOF OF THEOREMS

In this section, we provide mathematical proofs of the theorems.

### A. Proof of Theorem 1

Let $\eta_1 = 2\pi B([s_1/M_1] - [1/2])$, $\eta_1' = 2\pi B([s_1/M_1] - [3/2])$, $\eta_2 = 2\pi B([s_2/M_2] - [1/2] - [\tau/T_2])$, $\eta_2' = 2\pi B([s_1/M_1] - [3/2] - [\tau/T_2])$, and $\nu_i = (2\pi B/T_i)$, $i = 1, 2$. Then $x_1(t)$ and $x_2(t-\tau)$ can be written as

$$x_1(t) = \begin{cases} e^{j\left(\eta_1 t + \frac{\nu_1}{2}t^2\right)}, & 0 \le t < t_1 \\ e^{j\left(\eta_1' t + \frac{\nu_1}{2}t^2\right)}, & t_1 \le t < T_1 \end{cases} \tag{42}$$

$$x_2(t-\tau) = \begin{cases} Ae^{j\left(\eta_2 t + \frac{\nu_2}{2}t^2\right)}, & \tau \le t < t_2 + \tau \\ \mathcal{A}e^{j\left(\eta_2' t + \frac{\nu_2}{2}t^2\right)}, & t_2 + \tau \le t < T_2 + \tau \\ 0, & \text{otherwise.} \end{cases} \tag{43}$$

From (42) and (43), the cross-correlation between $x_1(t)$ and $x_2(t-\tau)$ can be calculated case by case for the following four cases (an illustrative example for these four cases is shown in Fig. 9).

*1) When $0 \le \tau \le t_1 - T_2$:* In this case, $x_1(t)$ for $0 \le t < t_1$ is first cross-correlated with $x_2(t-\tau)$ for $\tau \le t < t_2 + \tau$ over the range $\tau \le t < t_2 + \tau$, and then, is cross-correlated with $x_2(t-\tau)$ for $t_2 + \tau \le t < T_2 + \tau$ over the range $t_2 + \tau \le t < T_2 + \tau$. Thus, it follows that:

$$\rho(\tau; s_1, s_2) = \sqrt{\frac{1}{T_1 T_2}}\Bigg[A\int_{\tau}^{\tau+t_2} e^{j\left((\eta_2-\eta_1)t + \frac{\nu_2-\nu_1}{2}t^2\right)}dt + \mathcal{A}\int_{\tau+t_2}^{\tau+T_2} e^{j\left((\eta_2'-\eta_1)t + \frac{\nu_2-\nu_1}{2}t^2\right)}dt\Bigg]. \tag{44}$$

From Lemma 1 in Appendix B, it can be shown that the above integration is equivalent to the result of (8) for $0 \le \tau \le t_1 - T_2$.

*2) When $t_1 - T_2 < \tau \le t_1 - t_2$:* In this case, $x_1(t)$ for $0 \le t < t_1$ is first cross-correlated with $x_2(t-\tau)$ for $\tau \le t < t_2 + \tau$ over the range $\tau \le t < t_2 + \tau$, and then, is cross-correlated with $x_2(t-\tau)$ for $t_2 + \tau \le t < T_2 + \tau$ over the range $t_2 + \tau \le t < t_1$. Thereafter, $x_1(t)$ for $t_1 \le t < T_1$ is cross-correlated with $x_2(t-\tau)$ for $t_2 + \tau \le t < T_2 + \tau$ over the range $t_1 \le t < T_2 + \tau$. Thus, it follows that:

$$\begin{aligned}\rho(\tau; s_1, s_2) = \sqrt{\frac{1}{T_1 T_2}}\Bigg[A\int_{\tau}^{\tau+t_2} e^{j\left((\eta_2-\eta_1)t+\frac{\nu_2-\nu_1}{2}t^2\right)}dt \\ + \mathcal{A}\int_{\tau+t_2}^{t_1} e^{j\left((\eta_2'-\eta_1)t+\frac{\nu_2-\nu_1}{2}t^2\right)}dt \\ + \mathcal{A}\int_{t_1}^{\tau+T_2} e^{j\left((\eta_2'-\eta_1')t+\frac{\nu_2-\nu_1}{2}t^2\right)}dt\Bigg]. \end{aligned} \tag{45}$$

From Lemma 1 in Appendix B, it can be shown that the above integration is equivalent to the result of (8) for $t_1 - T_2 < \tau \le t_1 - t_2$.

*3) When $t_1 - t_2 < \tau \le t_1$:* In this case, $x_1(t)$ for $0 \le t < t_1$ is first cross-correlated with $x_2(t-\tau)$ for $\tau \le t < t_2 + \tau$ over the range $\tau \le t < t_1$. Then $x_1(t)$ for $t_1 \le t < T_1$ is cross-correlated with $x_2(t-\tau)$ for $\tau \le t < t_2+\tau$ over the range $t_1 \le t < t_2 + \tau$, followed by being cross-correlated with $x_2(t-\tau)$ for $t_2 + \tau \le t < T_2 + \tau$ over the range $t_2 + \tau \le t < T_2 + \tau$. Thus, it follows that:

$$\begin{aligned}\rho(\tau; s_1, s_2) = \sqrt{\frac{1}{T_1 T_2}}\Bigg[A\int_{\tau}^{t_1} e^{j\left((\eta_2-\eta_1)t+\frac{\nu_2-\nu_1}{2}t^2\right)}dt \\ + A\int_{t_1}^{\tau+t_2} e^{j\left((\eta_2-\eta_1')t+\frac{\nu_2-\nu_1}{2}t^2\right)}dt \\ + \mathcal{A}\int_{\tau+t_2}^{\tau+T_2} e^{j\left((\eta_2'-\eta_1')t+\frac{\nu_2-\nu_1}{2}t^2\right)}dt\Bigg]. \end{aligned} \tag{46}$$

From Lemma 1 in Appendix B, it can be shown that the above integration is equivalent to the result of (8) for $t_1 - t_2 < \tau \le t_1$.

*4) When $t_1 < \tau \le T_1 - T_2$:* In this case, $x_1(t)$ for $t_1 \le t < T_1$ is first cross-correlated with $x_2(t-\tau)$ for $\tau \le t < t_2 + \tau$ over the range $\tau \le t < t_2 + \tau$, and then, is cross-correlated with $x_2(t-\tau)$ for $t_2 + \tau \le t < T_2 + \tau$ over the range $t_2 + \tau \le t < T_2 + \tau$. Thus, it follows that:

$$\begin{aligned}\rho(\tau; s_1, s_2) = \sqrt{\frac{1}{T_1 T_2}}\Bigg[A\int_{\tau}^{\tau+t_2} e^{j\left((\eta_2-\eta_1')t+\frac{\nu_2-\nu_1}{2}t^2\right)}dt \\ + \mathcal{A}\int_{\tau+t_2}^{\tau+T_2} e^{j\left((\eta_2'-\eta_1')t+\frac{\nu_2-\nu_1}{2}t^2\right)}dt\Bigg]. \end{aligned} \tag{47}$$

From Lemma 1 in Appendix B, it can be shown that the above integration is equivalent to the result of (8) for $t_1 < \tau \le T_1 - T_2$.

## *B. Proof of Theorem 2*

For $y \ge 0$, it follows that $|F(z,y)|^2 \le (\max_w C(w))^2 + (\max_w S(w))^2$. Using this and applying the triangle inequality to the result of (8) for $t_1 - T_2 < \tau \le t_1 - t_2$ or $t_1 - t_2 < \tau \le t_1$, we get

$$\begin{aligned}|\rho(\tau; s_1, s_2)|^2 &\le \frac{3\Big[\big(\max_w C(w)\big)^2 + \big(\max_w S(w)\big)^2\Big]}{2(M_1 - M_2)} \\ &\approx \frac{1.677}{M_1 - M_2}\end{aligned} \tag{48}$$

where the last line follows since $\max_w C(w) \approx 0.78$ and $\max_w S(w) \approx 0.714$ [15].

## *C. Proof of Theorem 3*

Note that (24) is equivalent to

$$\begin{aligned}\varrho[m; s_1, s_2] &= \sqrt{\frac{1}{M_1 M_2}}\Lambda \sum_{n=m}^{M_2+m-1} e^{j2\pi\left(an^2+bn\right)} \\ &= \sqrt{\frac{1}{M_1 M_2}}\Lambda \sum_{n=0}^{M_2-1} e^{j2\pi\left(a(n+m)^2+b(n+m)\right)}\end{aligned} \tag{49}$$

where $a = (1/2)([1/M_2] - [1/M_2])$ and $b = ([s_2 - m]/M_2) - (s_1/M_1)$. By applying Lemma 2 in Appendix B to (49) with $q_n = 1$ and $\phi_n = 2\pi(a(n+m)^2 + b(n+m))$ for $n = 0, 1, \ldots, M_2 - 1$, it can be shown that $\varrho[m; s_1, s_2]$ can be expressed as in (25).

## *D. Proof of Theorem 4*

When $M_1 - 2M_2$, it follows that:

$$\begin{aligned}\varrho[m; s_1, s_2] &= \sqrt{\frac{1}{M_1 M_2}} \sum_{n=m}^{M_2+m-1} e^{j\pi\left(\frac{1}{M_2}-\frac{1}{M_1}\right)} e^{j2\pi\left(\frac{s_2-m}{M_2}-\frac{s_1}{M_1}\right)} \\ &= \sqrt{\frac{1}{M_1 M_2}} \sum_{n=0}^{M_2-1} e^{j\frac{\pi(n+m)^2}{2M_2}} e^{j\frac{2\pi i(n+m)}{M_2}} \\ &= \sqrt{\frac{1}{M_1 M_2}} e^{j\frac{\pi m^2}{2M_2}} e^{j\frac{2\pi i m}{M_2}} \sum_{n=0}^{M_2-1} e^{j\frac{\pi n^2}{2M_2}} e^{j\frac{2\pi kn}{M_2}}\end{aligned} \tag{50}$$

where $i = (s_2 - m - [M_2/M_1]s_1)_{\mathrm{mod} M_2}$ and $k = i + (m/2)_{\mathrm{mod} M_2}$. On the other hand, we have

$$\begin{aligned}&\sum_{n=0}^{M_2-1} e^{j\frac{\pi n^2}{2M_2}} e^{j\frac{2\pi kn}{M_2}} \\ &\quad= \sum_{n=0}^{M_2/2-1}\left[e^{j\frac{\pi(2n)^2}{2M_2}} e^{j\frac{2\pi k(2n)}{M_2}} + e^{j\frac{\pi(2n+1)^2}{2M_2}} e^{j\frac{2\pi k(2n+1)}{M_2}}\right] \\ &\quad= \underbrace{\sum_{n=0}^{M_2/2-1} e^{j\frac{\pi n^2}{M_2/2}} e^{j\frac{2\pi kn}{M_2/2}}}_{=\sqrt{\frac{M_2}{2}}e^{j\frac{\pi}{4}}e^{-j\frac{2\pi k^2}{M_2}}} \\ &\qquad + e^{j\frac{\pi(2k+1/2)n}{M_2}} \underbrace{\sum_{n=0}^{M_2/2-1} e^{j\frac{\pi n(n+1)}{M_2/2}} e^{j\frac{2\pi kn}{M_2/2}}}_{=-2e^{-j\frac{2\pi k(k+1)}{M_2}}\sum_{l=0}^{k-1} e^{j\frac{2\pi l(l+1)}{M_2}}}\end{aligned} \tag{51}$$

where the last line follows from Lemmas 5 and 6 in Appendix B. By substituting (51) into (52), the result of (28) can be obtained.

### E. Proof of Theorem 5

For fixed $M_2 < \infty$ and $m = o(M_1)$, when $M_1 \to \infty$ and $M_1 s_2 - M_2 s_1$ is a multiple of $M_1$, we have

$$\begin{aligned}\varrho[m; s_1, s_2] &= \sqrt{\frac{1}{M_1 M_2}} \sum_{n=m}^{M_2+m-1} e^{j\pi\left(\frac{1}{M_2}-\frac{1}{M_1}\right)} e^{j2\pi\left(\frac{s_2-m}{M_2}-\frac{s_1}{M_1}\right)} \\ &\to \sqrt{\frac{1}{M_1 M_2}} \sum_{n=m}^{M_2+m-1} e^{j\frac{\pi n^2}{M_2}} e^{j\frac{2\pi kn}{M_2}} \\ &= \sqrt{\frac{1}{M_1 M_2}} \underbrace{\sum_{n=0}^{M_2-1} e^{j\frac{\pi n^2}{M_2}} e^{j\frac{2\pi kn}{M_2}}}_{=\sqrt{M_2} e^{j\frac{\pi}{4}} e^{-j\frac{\pi k^2}{M_2}}} \end{aligned} \tag{52}$$

where $k = (s_2 - m - [M_2/M_1]s_1)_{\text{mod}M_2}$. Also, the last line follows from Lemma 5 in Appendix B and the fact that both $e^{j(\pi n^2/M_2)}$ and $e^{j(2\pi kn/M_2)}$ are periodic with period $M_2$. Thus, the result of (30) follows.

### F. Proof of Theorem 6

The result of (32) follows from the fact that $|\Lambda|^2 = |\exp(j\theta)|^2 = 1$ and $r^2 \le M_2(1 + 2\varepsilon)$.

### G. Proof of Theorem 7

The results of (35) follow since the upper bound of $|\rho(\tau; s_1, s_2)|^2$ in (19) and that of $|\varrho[m; s_1, s_2]|^2$ in (32) approach zero as $M_1 \to \infty$ with fixed $M_2 < \infty$ or as $M_2 \to \infty$ with fixed $(M_1/M_2) < \infty$.

## Appendix B
## List of Lemmas

In this Appendix, we list some lemmas that are useful for proving the theorems in this article.

*Lemma 1 (Integration of a Continuous-Time Chirp Signal Over a Finite Interval):* Suppose that $\nu > 0$. Then, it follows that:

$$\begin{aligned}&\int_u^v e^{j\left(\eta t + \frac{\nu}{2}t^2\right)} dt \\ &= \sqrt{\frac{\pi}{\nu}} e^{-j\frac{\eta^2}{2\nu}} \left[\big(C(V) - C(U)\big) + j\big(S(V) - S(U)\big)\right] \end{aligned} \tag{53}$$

where $U = \sqrt{(\nu/\pi)}(u + [\eta/\nu])$ and $V = \sqrt{(\nu/\pi)}(v + [\eta/\nu])$.

*Proof:* By completing the square of the bracketed term, we have

$$\begin{aligned}\int_u^v e^{j\left(\eta t+\frac{\nu}{2}t^2\right)} dt &= e^{-j\frac{\eta^2}{2\nu}} \int_u^v e^{j\frac{\nu}{2}\left(t+\frac{\eta}{\nu}\right)} dt \\ &= \sqrt{\frac{\pi}{\nu}} e^{-j\frac{\eta^2}{2\nu}} \int_U^V e^{j\frac{\pi z^2}{2}} dt \\ &= \sqrt{\frac{\pi}{\nu}} e^{-j\frac{\eta^2}{2\nu}} \left(\int_0^V e^{j\frac{\pi z^2}{2}} dt - \int_0^U e^{j\frac{\pi z^2}{2}} dt\right) \\ &= \sqrt{\frac{\pi}{\nu}} e^{-j\frac{\eta^2}{2\nu}} \left[C(V) + jS(V) - \big(C(U) + jS(U)\big)\right] \\ &= \sqrt{\frac{\pi}{\nu}} e^{-j\frac{\eta^2}{2\nu}} \left[\big(C(V) - C(U)\big) + j\big(S(V) - S(U)\big)\right] \end{aligned} \tag{54}$$

where in (54), we have changed the integration variable by letting $\sqrt{\nu}(t + [\eta/\nu]) = \sqrt{\pi} z$. ■

*Lemma 2 (Sum of N Complex Exponentials):* Suppose that there are $N$ complex exponentials with magnitudes $r_n$, $n = 0, \ldots, N-1$, and phases $\phi_n$, $n = 0, \ldots, N-1$. Then, it follows that:

$$\sum_{n=0}^{N-1} q_n e^{j\phi_n} = q e^{j\phi} \tag{55}$$

where

$$q = \sqrt{\sum_{n=0}^{N-1} q_n^2 + 2\sum_{n=0}^{N-1}\sum_{l=0}^{n-1} q_n q_m \cos(\phi_m - \phi_n)} \tag{56}$$

$$\phi = \tan^{-1}\left(\frac{\sum_{n=0}^{N-1} r_n \cos\phi_n}{\sum_{n=0}^{N-1} r_n \sin\phi_n}\right). \tag{57}$$

*Proof:* The summation can be equivalently written as

$$\sum_{n=0}^{N-1} q_n e^{j\phi_n} = \textstyle\sum_{n=0}^{N-1} q_n \cos\phi_n + j\sum_{n=0}^{N-1} q_n \sin\phi_n. \tag{58}$$

From (58), the phase of the summation can be determined as

$$\phi = \tan^{-1}\left(\frac{\sum_{n=0}^{N-1} r_n \cos\phi_n}{\sum_{n=0}^{N-1} r_n \sin\phi_n}\right). \tag{59}$$

Also, the squared magnitude of the summation can be determined as

$$\begin{aligned} q^2 &= \left(\sum_{n=0}^{N-1} q_n \cos\phi_n\right)^2 + \left(\sum_{n=0}^{N-1} q_n \sin\phi_n\right)^2 \\ &= \sum_{n=0}^{N-1}\left(q_n^2 \cos^2\phi_n + 2\sum_{l=0}^{n-1} q_n q_m \cos\phi_n \cos\phi_m\right) \\ &\quad + \sum_{n=0}^{N-1}\left(q_n^2 \sin^2\phi_n + 2\sum_{l=0}^{n-1} q_n q_m \sin\phi_n \sin\phi_m\right) \\ &= \sum_{n=0}^{N-1} q_n^2 + 2\sum_{n=0}^{N-1}\sum_{l=0}^{n-1} q_n q_m \cos(\phi_m - \phi_n). \end{aligned} \tag{60}$$

■

*Lemma 3 (Sum of a Discrete-Time Chirp Signal of Length N):* Suppose that $N$ is a positive even number. Then, it follows that:

$$\sum_{n=0}^{N-1} e^{j\frac{\pi n^2}{N}} = \sqrt{N} e^{j\frac{\pi}{4}}. \tag{61}$$

*Proof:* When $N \le 4$, we have

$$N = 2: \sum_{n=0}^{1} e^{j\frac{\pi n^2}{2}} = 1 + e^{j\frac{\pi}{2}} = \sqrt{2} e^{j\frac{\pi}{2}}$$

$$N = 4: \sum_{n=0}^{3} e^{j\frac{\pi n^2}{4}} = 1 + e^{j\frac{\pi}{2}} + \underbrace{e^{j\pi}}_{=-1} + \underbrace{e^{j\frac{9\pi}{2}}}_{=e^{j\frac{\pi}{2}}} = 2e^{j\frac{\pi}{2}}.$$

On the other hand, when $N \geq 8$, we have the following relationship:

$$\begin{aligned}\sum_{n=0}^{N-1} e^{j\frac{\pi n^2}{N}} &= \sum_{n=0}^{N/2-1}\left(e^{j\frac{\pi n^2}{N}} + e^{j\frac{\pi(n+N/2)^2}{N}}\right)\\ &= \sum_{n=0}^{N/2-1}\left(e^{j\frac{\pi n^2}{N}} + e^{j\frac{\pi n^2}{N}} e^{j\pi n}\underbrace{e^{j\frac{\pi N}{4}}}_{=1}\right)\\ &= \sum_{n=0}^{N/2-1} e^{j\frac{\pi n^2}{N}}\left(1+\underbrace{e^{j\pi n}}_{=(-1)^n}\right)\\ &= 2\sum_{n=0}^{N/4-1} e^{j\frac{\pi(2n)^2}{N}} = 2\sum_{n=0}^{N/4-1} e^{j\frac{\pi n^2}{N/4}}. \end{aligned} \tag{62}$$

Through recursive computations, we get

$$\begin{aligned} N=8:\ &\sum_{n=0}^{7} e^{j\frac{\pi n^2}{8}} = 2\sum_{n=0}^{1} e^{j\frac{\pi n^2}{2}} = 2^{3/2} e^{j\frac{\pi}{2}}\\ N=16:\ &\sum_{n=0}^{15} e^{j\frac{\pi n^2}{16}} = 2\sum_{n=0}^{3} e^{j\frac{\pi n^2}{4}} = 2^{4/2} e^{j\frac{\pi}{2}}\\ &\vdots \end{aligned}$$

Thus, it follows that:

$$\sum_{n=0}^{N-1} e^{j\frac{\pi n^2}{N}} = 2^{\frac{\log_2 N}{2}} e^{j\frac{\pi}{4}} = \sqrt{N} e^{j\frac{\pi}{4}}. \tag{63}$$

■

*Lemma 4 (Sum of a Discrete-Time Chirp Signal of Length N With Phase Shifts):* Suppose that $N$ is a positive even number. Then, it follows that:

$$\sum_{n=0}^{N-1} e^{j\frac{\pi n(n+1)}{N}} = 0. \tag{64}$$

*Proof:* The result can be proved as follows:

$$\begin{aligned}\sum_{n=0}^{N-1} e^{j\frac{\pi n(n+1)}{N}} &= \sum_{n=0}^{N/2-1}\left(e^{j\frac{\pi n(n+1)}{N}} + e^{j\frac{\pi(N-(n+1))(N-n)}{N}}\right)\\ &= \sum_{n=0}^{N/2-1}\left(e^{j\frac{\pi n(n+1)}{N}} + e^{j\frac{\pi n(n+1)}{N}}\underbrace{e^{j\pi N}}_{=1}\underbrace{e^{-j(2n+1)\pi}}_{=-1}\right)\\ &= \sum_{n=0}^{N/2-1} e^{j\frac{\pi n(n+1)}{N}}(1-1) = 0. \end{aligned}\tag{65}$$

■

*Lemma 5 (Discrete Fourier Transform of a Discrete-Time Chirp Signal of Length N):* Suppose that $N$ is a positive even number. Then, for an arbitrary integer $\kappa$, it follows that:

$$\sum_{n=0}^{N-1} e^{j\frac{\pi n^2}{N}} e^{j\frac{2\pi\kappa n}{N}} = \sqrt{N} e^{j\frac{\pi}{4}} e^{-j\frac{\pi k^2}{N}} \tag{66}$$

where $k \triangleq \kappa_{\text{mod}N}$.

*Proof:* The result can be proved as follows:

$$\begin{aligned}\sum_{n=0}^{N-1} e^{j\frac{\pi n^2}{N}} e^{j\frac{2\pi\kappa n}{N}} &= \sum_{n=0}^{N-1} e^{j\frac{\pi n^2}{N}} e^{j\frac{2\pi k n}{N}}\\ &= e^{-j\frac{\pi k^2}{N}}\sum_{n=0}^{N-1} e^{j\frac{\pi(n+k)^2}{N}}\\ &= e^{-j\frac{\pi k^2}{N}}\sum_{n=0}^{N-1} e^{j\frac{\pi n^2}{N}} \qquad (67)\\ &= \sqrt{N} e^{j\frac{\pi}{4}} e^{-j\frac{\pi k^2}{N}} \qquad (68)\end{aligned}$$

where (67) follows since $e^{j(\pi n^2/N)} = e^{j([\pi(n+N)^2]/N)}$ for an even $N$ and (68) follows from Lemma 3. ■

*Lemma 6 (Discrete Fourier Transform of a Discrete-Time Chirp Signal of Length N With Phase Shifts):* Suppose that $N$ is a positive even number. Then, for an arbitrary integer $\kappa$, it follows that:

$$\sum_{n=0}^{N-1} e^{j\frac{\pi n(n+1)}{N}} e^{j\frac{2\pi\kappa n}{N}} = \begin{cases} 0, & k=0\\ -2e^{-j\frac{\pi k(k+1)}{N}}\sum_{l=0}^{k-1} e^{j\frac{\pi l(l+1)^2}{N}}, & \text{otherwise}\end{cases} \tag{69}$$

where $k \triangleq \kappa_{\text{mod}N}$.

*Proof:* The result when $\kappa = 0$ follows directly from Lemma 5. So, we focus on the proof when $\kappa \neq 0$

$$\begin{aligned}\sum_{n=0}^{N-1} e^{j\frac{\pi n(n+1)}{N}} e^{j\frac{2\pi\kappa n}{N}} &= \sum_{n=0}^{N-1} e^{j\frac{\pi n(n+1)}{N}} e^{j\frac{2\pi k n}{N}}\\ &= e^{-j\frac{\pi k(k+1)}{N}}\sum_{l=k}^{N+k-1} e^{j\frac{\pi l(l+1)}{N}}\\ &= e^{-j\frac{\pi k(k+1)}{N}}\left[\sum_{l=k}^{N-1} e^{j\frac{\pi l(l+1)}{N}} - \sum_{l=0}^{k-1} e^{j\frac{\pi l(l+1)}{N}}\right] \qquad (70)\\ &= -2e^{-j\frac{\pi k(k+1)}{N}}\sum_{l=0}^{k-1} e^{j\frac{\pi l(l+1)^2}{N}} \qquad (71)\end{aligned}$$

where (70) follows since $e^{j([\pi(l+N)(l+N+1)]/N)} = -e^{j([\pi l(l+1)]/N)}$, and thus, $\sum_{l=N}^{N+k-1} e^{j([\pi l(l+1)]/N)} = -\sum_{l=0}^{k-1} e^{j([\pi l(l+1)]/N)}$. Also, (71) follows by Lemma 4 as

$$\begin{aligned}\sum_{l=k}^{N-1} e^{j\frac{\pi l(l+1)}{N}} &= \underbrace{\sum_{l=0}^{N-1} e^{j\frac{\pi l(l+1)}{N}}}_{=0} - \sum_{l=0}^{k-1} e^{j\frac{\pi l(l+1)}{N}}\\ &= -\sum_{l=0}^{k-1} e^{j\frac{\pi l(l+1)}{N}}. \end{aligned}\tag{72}$$

■

## REFERENCES

[1] A. Al-Fuqaha, M. Guizani, M. Mohammadi, M. Aledhari, and M. Ayyash, "Internet of Things: A survey on enabling technologies, protocols, and applications," *IEEE Commun. Surveys Tuts.*, vol. 17, no. 4, pp. 2347–2376, 4th Quart., 2015.

[2] U. Raza, P. Kulkarni, and M. Sooriyabandara, "Low power wide area networks: An overview," *IEEE Commun. Surveys Tuts.*, vol. 19, no. 2, pp. 855–873, 2nd Quart., 2017.

[3] R. Ghanaatian, O. Afisiadis, M. Cotting, and A. Burg, "LoRa digital receiver analysis and implementation," in *Proc. IEEE ICASSP*, 2019, pp. 1498–1502.

[4] M. Xhonneux, O. Afisiadis, D. Bol, and J. Louveaux, "A low-complexity LoRa synchronization algorithm robust to sampling time offsets," *IEEE Internet Things J.*, vol. 9, no. 5, pp. 3756–3769, Mar. 2022.

[5] C. Bernier, F. Dehmas, and N. Deparis, "Low complexity LoRa frame synchronization for ultra-low power software-defined radios," *IEEE Trans. Commun.*, vol. 68, no. 5, pp. 3140–3152, May 2020.

[6] M. Chiani and A. Elzanaty, "On the LoRa modulation for IoT: Waveform properties and spectral analysis," *IEEE Internet Things J.*, vol. 6, no. 5, pp. 8463–8470, Oct. 2019.

[7] J. Petäjäjärvi, K. Mikhaylov, M. Pettissalo, J. Janhunen, and J. Iinatti, "Performance of a low-power wide-area network based on LoRa technology: Doppler robustness, scalability, and coverage," *Int. J. Distrib. Sens. Netw.*, vol. 13, no. 3, pp. 1–16, 2017.

[8] B. Reynders and S. Pollin, "Chirp spread spectrum as a modulation technique for long range communication," in *Proc. Symp. Commun. Veh. Technol.*, Nov. 2016, pp. 1–5.

[9] O. Georgiou and U. Raza, "Low power wide area network analysis: Can LoRa scale?" *IEEE Wireless Commun. Lett.*, vol. 6, no. 2, pp. 162–165, Apr. 2017.

[10] O. Afisiadis, S. Li, J. Tapparel, A. Burg, and A. Balatsoukas-Stimming, "On the advantage of coherent LoRa detection in the presence of interference," *IEEE Internet Things J.*, vol. 8, no. 14, pp. 11581–11593, Jul. 2021.

[11] L. Vangelista, "Frequency shift chirp modulation: The LoRa modulation," *IEEE Signal Process. Lett.*, vol. 24, no. 12, pp. 1818–1821, Dec. 2017.

[12] M. Hanif and H. H. Nguyen, "Slope-shift keying LoRa-based modulation," *IEEE Internet Things J.*, vol. 8, no. 1, pp. 211–221, Jan. 2021.

[13] D. Croce, M. Gucciardo, S. Mangione, G. Santaromita, and I. Tinnirello, "Impact of LoRa imperfect orthogonality: Analysis of link-level performance," *IEEE Commun. Lett.*, vol. 22, no. 4, pp. 796–799, Apr. 2018.

[14] D. Croce, M. Gucciardo, S. Mangione, G. Santaromita, and I. Tinnirello, "LoRa technology demystified: From link behavior to cell-level performance," *IEEE Trans. Wireless Commun.*, vol. 19, no. 2, pp. 822–834, Feb. 2020.

[15] M. Abramowitz and I. A. Stegun, *Handbook of Mathematical Functions With Formulas, Graphs, and Mathematical Tables*, vol. 55. New York, NY, USA: Dover, 1974.


**Jae-Mo Kang** (Member, IEEE) received the Ph.D. degree in electrical engineering from Korea Advanced Institute of Science and Technology, Daejeon, South Korea, in 2017.

He was a Postdoctoral Fellow with the Department of Electrical and Computer Engineering, Queen's University, Kingston, Canada, and an Assistant Professor with the School of Intelligent Mechatronics Engineering, Sejong University, Seoul, South Korea. He is currently an Assistant Professor with the Department of Artificial Intelligent, Kyungpook National University, Daegu, South Korea. His research interests include learning theory, training design, computer vision, IoT/LoRa/6G, and UAV/Drone.

**Dong-Woo Lim** received the Ph.D. degree in electrical engineering from Korea Advanced Institute of Science and Technology, Daejeon, South Korea, in 2019.

He is currently with the Radio and Satellite Research Division, Electronics and Telecommunications Research Institute, Daejeon. His current research interests include Internet of Things, device-to-device communications, energy harvesting, relay networks, deep learning, and deep reinforcement learning.